

Speciation of adsorbed yttrium and rare earth elements on oxide surfaces

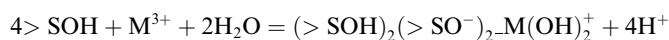
Wojciech Piasecki, Dimitri A. Sverjensky^{*,1}

Department of Earth and Planetary Sciences, The Johns Hopkins University, Baltimore, MD 21218, USA

Received 20 November 2007; accepted in revised form 29 May 2008; available online 10 June 2008

Abstract

The distribution of yttrium and the rare earth elements (YREE) between natural waters and oxide mineral surfaces depends on adsorption reactions, which in turn depend on the specific way in which YREE are coordinated to mineral surfaces. Recent X-ray studies have established that Y^{3+} is adsorbed to the rutile (110) surface as a distinctive tetranuclear species. However, the hydrolysis state of the adsorbed cation is not known from experiment. Previous surface complexation models of YREE adsorption have suggested two to four cation hydrolysis states coexisting on oxide surfaces. In the present study, we investigate the applicability of the X-ray results to rare earth elements and to several oxides in addition to rutile using the extended triple-layer surface complexation model. The reaction producing a hydrolyzed tetranuclear surface species



was found to account for a significant fraction of the adsorbed Y^{3+} , La^{3+} , Nd^{3+} , Gd^{3+} , and Yb^{3+} on rutile, hematite, alumina and silica over wide ranges of pH and ionic strength. Where adsorption data were available as a function of surface coverage for hematite and silica, an additional reaction involving a mononuclear species could be used to account for the higher surface coverages. However, it is also possible that some of the higher surface coverage data refer to surface precipitation rather than adsorption. The results of the present study provide an internally consistent basis for describing YREE adsorption which could be used to investigate more complex systems in which YREE compete both in aqueous solution and on mineral surfaces with alkaline earths and ligands such as carbonate, sulfate, chloride and organic species, in order to build a predictive adsorption model applicable to natural waters.

© 2008 Elsevier Ltd. All rights reserved.

1. INTRODUCTION

The relative abundances of yttrium and the rare earth elements (YREE) are widely used tracers of geochemical processes. For surficial conditions, there is considerable interest in using YREE patterns of minerals and natural waters to decipher water–rock interactions in streams, soils, aquifers and mines (Sholkovitz, 1992; Bau et al., 2004;

Verplanck et al., 2004; Gammons et al., 2005; Tang and Johannesson, 2005) and to interpret the chemistry of seawater at the present and in the geologic past (Bau, 1999; Ohta and Kawabe, 2001; Byrne, 2002; Koschinsky and Hein, 2003; Davranche et al., 2004; Haley et al., 2004; Johannesson et al., 2006). It is likely that minerals take up YREE from aqueous solutions through a variety of scavenging processes including adsorption, the formation of surface solid solutions, and surface precipitation (Farley et al., 1985; Schindler and Stumm, 1987; Katz and Hayes, 1995; Dardenne et al., 2002). However, a principal mechanism governing YREE patterns in such systems is adsorption (Quinn et al., 2006a,b). The distribution of YREE between natural waters and oxide mineral surfaces depends on adsorption reactions.

* Corresponding author. Fax: +1 410 516 7933.

E-mail address: sver@jhu.edu (D.A. Sverjensky).

¹ Present address: Group for Theoretical Problems of Adsorption, Institute of Catalysis and Surface Chemistry, Polish Academy of Sciences, ul. Niezapominajek 8, 30-239 Kraków, Poland.

Experimental studies of YREE adsorption have demonstrated that, like all metal adsorption reactions, the adsorption of YREE depends on environmental variables such as pH, ionic strength, temperature, the presence of additional ligands such as carbonate or organic species, and surface coverage (Music and Ristic, 1988; Koepenkastrup and De Carlo, 1992; Kosmulski, 1997; Marmier et al., 1997, 1999a,b; De Carlo et al., 1998; Rabung et al., 1998; Marmier and Fromage, 1999; Coppin et al., 2002; Davranche et al., 2004, 2005; Kowal-Fouchard et al., 2004; Yoshida et al., 2004; Zhang et al., 2004b; Ridley et al., 2005; Tang and Johannesson, 2005; Quinn et al., 2006a,b, 2007). In addition, there are indications of a dependence on the type of oxide mineral (Byrne and Kim, 1990; Ohta and Kawabe, 2001; Quinn et al., 2004), as well as effects specific to the characteristics of the different rare earth elements (Bau, 1999; Ohta and Kawabe, 2000; Tao et al., 2004). The dependence on environmental variables results from the interfacial chemical reactions associated with adsorption in the electric field at the oxide–water interface. In turn, the interfacial reactions depend on the structure of the interface. More specifically, they depend on how YREE are attached to oxide mineral surfaces. In other words, what are the surface species of YREE? The dependence on the type of oxide mineral is almost certainly also related to the structure of the interface, through the specific role played by water molecules of solvation as YREE approach the surface. If this effect is taken into account, recent studies have shown that it becomes possible to place the adsorption of metals and oxyanions on a predictive basis (Sverjensky, 2005, 2006; Sverjensky and Fukushi, 2006; Fukushi and Sverjensky, 2007a).

Direct evidence of the surface speciation of YREE on oxide and silicate minerals has come from recent advances in synchrotron-based X-ray studies (Dardenne et al., 2002; Kowal-Fouchard et al., 2004; Zhang et al., 2004a,b). In particular, the application of X-ray standing-wave techniques to the rutile (110)–electrolyte–water interface has provided an extremely detailed picture of the structure of the interface for adsorbed Rb^+ , Sr^{2+} , Zn^{2+} , and Y^{3+} in NaCl solutions free of carbonate (Zhang et al., 2004b, 2006a,b). Three general results follow from these studies. First, divalent cations with very different sizes form different surface species. Second, a given cation can form more than one type of surface species. Third, the three larger cations, Rb^+ , Sr^{2+} , and Y^{3+} , all occupy an inner-sphere tetranuclear site at the rutile (110) surface (Sr^{2+} also forms an outer-sphere species under some conditions). The tetranuclear site is shown in Fig. 1, where Y^{3+} binds to two bridging oxygens and two singly-coordinated oxygens which belong to four different underlying metal polyhedra near the rutile surface. By analogy with these results, it can be expected that the REE will also bind to this site on the rutile (110) surface (Ridley et al., 2005). The applicability of these results to other solids has not yet been investigated. Furthermore, the X-ray results do not yield information on the protonation state of the adsorbed species. As shown schematically in Fig. 1, the Y^{3+} could also be coordinated to three O, OH, or H_2O ligands away from the surface. In the absence of experimental or theoretical evidence, the state of hydrolysis and stoichiometry of the adsorption

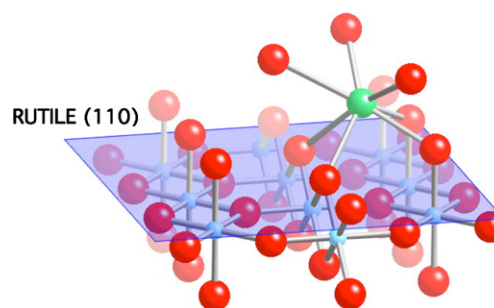


Fig. 1. Schematic representation of Y^{3+} adsorbed to the rutile (110) surface (after Zhang et al., 2004b). The Y^{3+} occupies a tetranuclear surface site where it is bonded to two bridging oxygens and two terminal oxygens of the rutile. It is assumed here that the Y^{3+} is also bonded to three water or hydroxyl species away from the surface (shown as oxygens). Surface complexation modeling reported here indicates that two of these could be hydroxyl species.

reactions for YREE on rutile and other solids must be defined through indirect means with surface complexation models of macroscopic proton surface titration and adsorption data.

Surface complexation models of REE adsorption and scavenging experiments have employed a variety of adsorption reactions and model assumptions (Marmier et al., 1997, 1999a,b; Rabung et al., 1998; Marmier and Fromage, 1999; Ridley et al., 2005; Tang and Johannesson, 2005; Quinn et al., 2006a,b). The models vary enormously in their assumptions and complexity. Only the model for Nd^{3+} adsorbed on rutile in NaCl solutions (Ridley et al., 2005) used tetranuclear surface species consistent with the X-ray studies summarized above. In this approach, a multisite model with a three-plane description of the electric double-layer structure was developed. It included four reaction stoichiometries for Nd^{3+} adsorption, differing in the hydration state of the surface Nd^{3+} species. The four different Nd–OH surface species accounted for adsorption and surface protonation data over a wide range of pH values, ionic strengths, and temperatures. However, only a single surface coverage was modeled. Consequently, it remains to be established whether tetranuclear species for YREE can account for adsorption data referring to a range of surface coverages and oxides other than rutile.

In contrast to the Nd^{3+} study, a study of Y^{3+} and all the REE which involved scavenging of the metals by precipitating ferric hydroxide over a wide range of pH, ionic strength, surface coverage and carbonate concentrations (Quinn et al., 2006a,b), was able to account for the experimental data using a relatively simple surface complexation model. It involved three reaction stoichiometries containing mononuclear surface species, i.e. binding of YREE to oxygen coordinated to a single underlying metal polyhedron. Two of the reactions differed only in the hydrolysis state of the adsorbed metal, and a third reaction involving a ternary carbonate surface complex. However, an electric double-layer was not included in the model. This could limit the applicability of the model to systems in which the main electrolyte has strongly different characteristics. At present, there is no single, internally consistent, surface complexation model of YREE adsorption applicable to a wide

variety of solids and environmental conditions that is also consistent with the results of the X-ray studies.

The purpose of the present study is to establish a simple, internally consistent surface complexation model of YREE adsorption that includes an electric double-layer and is applicable to a wide variety of solids and environmental conditions. We investigate the applicability of the tetranuclear Y^{3+} surface species on rutile (110) established by the X-ray studies to adsorption studies of the REE on other oxides. Our study is analogous to a previously published surface complexation analysis of the alkaline earths based on X-ray results for Sr^{2+} on the (110) surface of rutile (Sverjensky, 2006). Emphasis is placed on the analysis of adsorption, surface protonation, and proton coadsorption experiments referring to a wide range of pH, ionic strength, surface coverage and oxide types with an electric double-layer model. The goals of the simulations are to determine whether one or more than one reaction stoichiometry is needed, the state of hydrolysis of the adsorbed cation, and whether different oxide minerals share common reaction stoichiometries.

It should be noted here that a surface complexation analysis cannot establish a model for the total coordination number of the adsorbed cation. For example, a coordination number of seven is depicted in Fig. 1, based on the known preference of YREE to have coordination numbers of at least seven in silicate and phosphate minerals (Smyth and Bish, 1988). Similarly, Lu sorbed onto ferrihydrite had a coordination number of seven (Dardenne et al., 2001). It is possible that the coordination number of the Y in Fig. 1 should be even higher. YREE coordinate to 8–9 water molecules in aqueous solution (Rizkalla and Choppin, 1991; Ragnarsdottir et al., 1998; Ridley et al., 2005). Also, a value of eight was indicated by molecular modeling for Sr^{2+} on rutile (Zhang et al., 2004b). The Sr^{2+} had a coordination similar to that shown in Fig. 1, but with an additional bond to the oxygen directly below it in the plane of Ti atoms. However, surface complexation only establishes a model of the adsorption reaction stoichiometry. This is sensitive to the number of linkages to polyhedra on the surface (i.e. four in Fig. 1 as determined by X-ray analysis) and the number of hydroxyl groups coordinated to the adsorbed cation (not explicitly shown in Fig. 1). The number of waters coordinated to the adsorbed cation cannot currently be established by surface complexation modeling.

The present study is restricted to the analysis of experiments designed to study adsorption processes only. The scavenging experiments for YREE are not analyzed here. However, the results of the present study will serve as a basis for assessing the applicability of electrochemical models of adsorption to the hydrous ferric hydroxide scavenging experiments, which may involve processes in addition to adsorption. The results of the present study can be combined with previous internally consistent studies emphasizing a predictive surface complexation approach for the adsorption of protons, alkalis, alkaline earths, halide anions and oxyanions (Sverjensky and Fukushi, 2006; Fukushi and Sverjensky, 2007a,b; Sverjensky, 2001, 2003, 2005, 2006). In this way, it becomes possible to build a model with which competitive adsorption (e.g. Ca^{2+} or Mg^{2+} vs. YREE) or ternary surface complex formation can be ana-

lyzed. Such an approach should be useful in helping to analyze YREE adsorption in experimental and natural systems with a great variety of solution compositions.

2. ANALYSIS OF ADSORPTION AND PROTON SURFACE CHARGE DATA

2.1. Modeling approach, assumptions and uncertainties

The approach used in the present study builds on the predictive single-site triple-layer model and associated crystal chemical and Born solvation theory referred to as the extended triple-layer model (ETLM, Sverjensky, 2005, 2006). In the triple-layer model, protons are assumed to adsorb at a near surface plane, the 0-plane, and electrolyte ions are assumed to adsorb at the β -plane slightly further away from the surface. The potentials and charges at these planes are represented by ψ_0 , ψ_β , and σ_0 , σ_β , respectively. The change in potential from the 0- to the β -plane is expressed in the capacitance (C_1). All the experimental adsorption and surface protonation data in the presence of YREE analyzed here refer to systems containing an oxide powder in a single background electrolyte. The oxide sample characteristics can be interpreted as referring to an averaging over all crystallographic planes and sites. Accordingly, the BET surface area (A_s), the surface protonation equilibrium constants, electrolyte adsorption equilibrium constants, capacitances, and site densities (i.e. the number of adsorption sites per nm^{-2} , N_s) are given in Table 1. Where possible, these were constrained by experiment, otherwise they were obtained using the predictive approach summarized in Sverjensky (2005) as noted in Table 1. Hydrolysis and aqueous complexing of YREE was treated using equilibrium constants taken from the literature (Klungness and Byrne, 2000; Luo and Byrne, 2001).

The principal assumption of the surface complexation modeling is that the adsorption reactions used for YREE should include a tetranuclear surface species, as indicated by the X-ray studies for rutile described above. In turn, this assumes that there is a potential tetranuclear site available on solids other than rutile. In principle, there are many possible reactions producing tetranuclear species. These differ in the number of charged surface sites coordinated to the adsorbed metal and in the state of hydrolysis of the adsorbed metal. As in the case of the heavy alkaline earths (Sverjensky, 2006), two charged and two neutral sites per adsorbed metal were found to be the most useful. An example of such a species is $(>SOH)_2(>SO^-)_2M^{3+}$, where the adsorbed metal is on the β -plane of the model. However, there are a number of possible reactions involving similar species which differ only in their hydrolysis state. These include

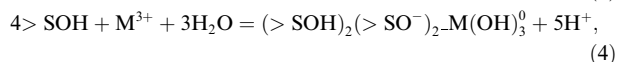
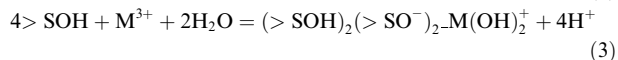
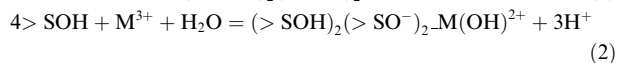
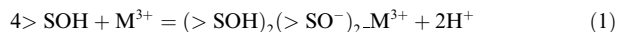
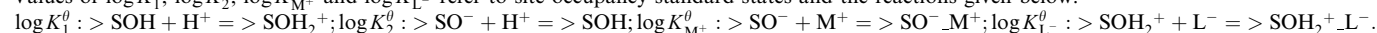


Table 1
Sample characteristics and extended triple-layer model parameters for proton and 1:1 electrolyte adsorption

Solid	N_s (sites nm^{-2})	A_s ($\text{m}^2 \text{g}^{-1}$)	pH_{ZPC}	$\Delta\text{p}K_n^0$	$\log K_1^0$	$\log K_2^0$	$\log K_1^0$	$\log K_2^0$	Salt (ML)	$\log^* K_{\text{M}^+}^0$	$\log^* K_{\text{L}^-}^0$	$\log K_{\text{M}^+}^0$	$\log K_{\text{L}^-}^0$	C_1 ($\mu\text{F cm}^{-2}$)
$\alpha - \text{TiO}_2^{\text{a}}$	12.5	14.7	5.4	6.3	2.2	8.6	1.9	8.9	NaCl	-6.1	4.6	2.8	2.7	120
$\alpha - \text{TiO}_2^{\text{b}}$	12.5	16.9	5.4	6.3	2.2	8.6	1.9	8.9	NaCl	-6.1	4.6	2.8	2.7	120
$\text{Fe}_3\text{O}_4^{\text{c}}$	6.0	1.8	6.3	5.7	3.5	9.2	4.5	8.2	NaNO_3	-6.2	7.1	2.0	2.7	130
$\text{Al}_2\text{O}_3^{\text{d}}$	8.0	135	8.6	5.9	5.6	11.6	4.6	12.6	NaNO_3	-9.7	7.5	3.0	2.8	100
$\text{Al}_2\text{O}_3^{\text{e}}$	8.0	155	8.8	5.9	5.8	11.7	4.8	12.8	NaClO_4	-9.8	6.9	3.0	2.1	100
$\text{Fe}_2\text{O}_3^{\text{f}}$	22.0	8.5	8.1	5.5	5.3	10.9	5.1	11.1	NaNO_3	-9.2	6.8	1.9	1.7	70
$\text{am-SiO}_2^{\text{g}}$	4.6	384.0	2.8	8.4	-1.4	7.0	-2.6	8.2	NaNO_3	-7.1	-0.9	1.1	1.7	95

Values of $\log K_1^0$, $\log K_2^0$, $\log K_{\text{M}^+}^0$ and $\log K_{\text{L}^-}^0$ refer to site-occupancy standard states and the reactions given below:



Values of $\log K_1^0$, $\log K_2^0$, $\log^* K_{\text{M}^+}^0$ and $\log^* K_{\text{L}^-}^0$ refer to the hypothetical 1.0 M standard state and the reactions given below:

$\log K_1 : > \text{SOH} + \text{H}^+ = > \text{SOH}_2^+; \log K_2^0 : > \text{SO}^- + \text{H}^+ = > \text{SOH}; \log^* K_{\text{M}^+}^0 : > \text{SOH} + \text{M}^+ = > \text{SO}^- \text{M}^+ + \text{H}^+; \log^* K_{\text{L}^-}^0 : > \text{SOH} + \text{H}^+ + \text{L}^- = > \text{SOH}_2^+ \text{L}^-$. The parameters $\log^* K_{\text{M}^+}^0$, $\log^* K_{\text{L}^-}^0$, and C_1 were generated by regression of proton surface charge data as noted. Otherwise, $\log^* K_{\text{M}^+}^0$ and $\log^* K_{\text{L}^-}^0$ were calculated from the values of $\log K_{\text{M}^+}^0$, $\log K_{\text{L}^-}^0$, pH_{ZPC} , $\Delta\text{p}K_n^0$, N_s , and A_s using equations in Sverjensky (2005) and C_1 was predicted (Sverjensky, 2005). Values of N_s and $\Delta\text{p}K_n^0$ were taken from Sverjensky (2005). Values of A_s represent experimental BET surface areas from the studies cited. Values of pH_{ZPC} were predicted theoretically or taken from the experimental sources cited.

^a $\log^* K_{\text{M}^+}^0$, $\log^* K_{\text{L}^-}^0$, and C_1 from regression calculations reported in Sverjensky (2005), BET surface area from Zhang et al. (2004b).

^b $\log^* K_{\text{M}^+}^0$, $\log^* K_{\text{L}^-}^0$, and C_1 from regression calculations reported in Sverjensky (2005), BET surface area from Ridley et al. (2005).

^c $\log^* K_{\text{M}^+}^0$ and C_1 from regression of proton surface charge data reported in Marmier et al. (1999b), see text.

^d All parameters predicted, except for the BET surface area from Marmier et al. (1997).

^e All parameters predicted, except for the BET surface area from Kosmulski (1997).

^f $\log^* K_{\text{M}^+}^0$, $\log^* K_{\text{L}^-}^0$ and C_1 from regression of proton surface charge data reported in Marmier and Fromage (1999).

^g $\log^* K_{\text{M}^+}^0$ and C_1 from regression of proton surface charge data reported in Marmier et al. (1999a).

all of which are consistent with the experimental X-ray studies.

The corresponding equilibrium constants are given by

$$\log^* K_{M^{3+}}^{\theta} = \frac{a_{(>SOH)_2(>SO^-)_2-M^{3+}} a_{H^+}^2}{a_{>SOH}^4 a_{M^{3+}}} 10^{\frac{F(3\psi_{\beta}-2\psi_0)}{2.303RT}} \quad (5)$$

$$\log^* K_{M(OH)^{2+}}^{\theta} = \frac{a_{(>SOH)_2(>SO^-)_2-M(OH)^{2+}} a_{H^+}^3}{a_{>SOH}^4 a_{M^{3+}} a_{H_2O}} 10^{\frac{F(2\psi_{\beta}-2\psi_0)}{2.303RT}} \quad (6)$$

$$\log^* K_{M(OH)_2^+}^{\theta} = \frac{a_{(>SOH)_2(>SO^-)_2-M(OH)_2^+} a_{H^+}^4}{a_{>SOH}^4 a_{M^{3+}} a_{H_2O}^2} 10^{\frac{F(\psi_{\beta}-2\psi_0)}{2.303RT}} \quad (7)$$

$$\log^* K_{M(OH)_3^0}^{\theta} = \frac{a_{(>SOH)_2(>SO^-)_2-M(OH)_3^0} a_{H^+}^5}{a_{>SOH}^4 a_{M^{3+}} a_{H_2O}^3} 10^{\frac{F(2\psi_0)}{2.303RT}} \quad (8)$$

where the superscripts “*” and “ θ ” refer to reactions written relative to $>SOH$, and to site-occupancy standard states (Sverjensky, 2003), respectively.

Previous surface complexation studies of YREE used combinations of two to four adsorption reactions similar to Eqs. (1)–(4), i.e. involving hydrolysis of trivalent YREE on mineral surfaces. This implies multiple metal hydroxy species on the surface. Distinguishing between these reactions is greatly facilitated with surface protonation data (Ridley et al., 2005). In the present study we take advantage of this surface protonation and adsorption data for YREE to choose among the reactions in Eqs. (1)–(4) in the context of the ETLM and to compare the results with those of previous studies (see below).

The assessment of uncertainties in experimental adsorption studies is often not provided. For metal uptake experiments, uncertainties are largest at the lowest percentages adsorbed and may be of the order of ± 5 –10% (see below). For proton surface charge studies an uncertainty of $\pm 0.5 \mu C cm^{-2}$ has been cited (Yates and Healy, 1980). Unless otherwise stated these uncertainties have been used as a guide in the analysis discussed below, resulting in an overall uncertainty for the values of $\log K$ for YREE of about ± 0.2 . Regression calculations were carried out iteratively to investigate the applicability of the reactions in Eqs. (1)–(4) over a wide range of experimental conditions and types of oxide. Where a single adsorption reaction significantly underestimated the amount of adsorption, additional reaction stoichiometries were investigated. In addition, we checked the expected pH limits for precipitation of $M(OH)_3$ solids using equilibrium constants from the literature (Baes and Mesmer, 1976).

The regression calculations discussed below generated values of the equilibrium constants for YREE adsorption represented by $\log^* K_M^0$ in Table 2. The superscript “0” represents the hypothetical 1.0 M standard state (Sverjensky, 2003). These values were converted to values of $\log K_M^{\theta}$ referring to site-occupancy standard states and referenced to $>SO^-$ using the equations in Appendix A, together with the values of N_s (site density), A_s (BET surface area), pH_{ZPC} (the pristine point of zero charge equal to $0.5(\log K_1^{\theta} + \log K_2^{\theta})$), and ΔpK_n^{θ} (equal to $\log K_2^{\theta} - \log K_1^{\theta}$) given in Table 1. It is the values of $\log K_M^{\theta}$ in Table 2 that are independent of the individual sample characteristics, and therefore useful for comparing the binding of YREE on different oxides.

2.2. Y^{3+} and Nd^{3+} on rutile

Adsorption and surface protonation data for Y^{3+} and Nd^{3+} on rutile in NaCl solutions at two ionic strengths are represented by the symbols in Figs. 2 and 3 (Zhang et al., 2004b; Ridley et al., 2005). The surface coverages at 100% adsorption would be 1.9 and $1.8 \mu mol m^{-2}$, respectively. The solid curves in the figures represent regression calculations. Both datasets are noteworthy for the steep adsorption edges beginning at pH values less than pH_{ZPC} (5.4) and the small dependence on ionic strength. During the course of the measurements, the pH was changed by the addition of sufficient titrant to cause a progressive dilution of the initial YREE concentration. As a consequence, the data do not represent constant overall YREE or solid concentrations. In the present study, in order to facilitate the computation of model curves, a uniform set of average YREE and solid concentrations were adopted as noted on the figures. Values were chosen to approximate the steepest most rapidly changing parts of the data (i.e. the mid-points at pH values of about 5–6). These approximations can lead to discrepancies of the order of about $\pm 3 \mu C cm^{-2}$ in model curves relative to the experimental data.

Despite the approximations necessary to generate the model curves, the combination of surface protonation and adsorption data are extremely valuable in choosing between the reactions in Eqs. (1)–(4). For example, it can be seen in Fig. 2 that the surface protonation data for Y^{3+} on rutile enable a choice of which reaction is closest to describing the experimental data at a single surface coverage in the context of the ETLM. Clearly, it is only the reaction involving the dihydroxy surface species $(>SOH)_2(>SO^-)_2-Y(OH)_2^+$ (Fig. 2E and F) that can describe the experimental data. The model curves in Fig. 2F show relatively small discrepancies with the experimental data within about $\pm 5 \mu C cm^{-2}$. The model curves for the other reactions depicted in Fig. 2 resulted in discrepancies far outside the uncertainties of the present approach and the experimental data.

In Fig. 3 it can be seen that the reaction stoichiometry established above for Y^{3+} also applies to the surface protonation data for Nd^{3+} on rutile. Other reaction stoichiometries are not shown in this figure, but it can be seen that the reaction involving $(>SOH)_2(>SO^-)_2-Nd(OH)_2^+$ (Eq. (3)) is closely consistent with the experimental data except for a systematic discrepancy at the highest pH values at low ionic strength. The cause of this discrepancy is not clear, because under these conditions all the Nd^{3+} appears to be adsorbed to the surface. However, a similar discrepancy between model curve and experimental data was obtained using a Stern-based MUSIC model of these data (Ridley et al., 2005).

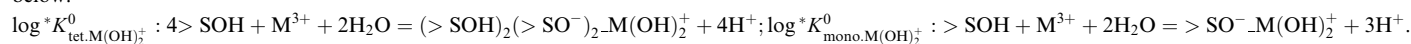
Overall, the results shown in Figs. 2 and 3 strongly support the choice of the reaction in Eq. (3), i.e. formation of a dihydroxy surface species of the type $(>SOH)_2(>SO^-)_2-M(OH)_2^+$. In the calculations reported below we investigated the applicability of Eq. (3) to a range of surface coverages and a variety of oxide adsorbates. It should be emphasized that the reaction stoichiometry used here is specific to the ETLM. Previous surface complexation studies have also used reactions involving hydrolysis of the adsorbed

Table 2

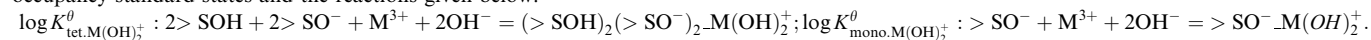
Equilibrium constants for YREE adsorption on oxides

Solid	M	$\log^* K_{M(\text{OH})_2^+}^{\text{tet.}}$	$\log^* K_{M(\text{OH})_2^+}^{\text{mono.}}$	N_s (sites nm^{-2})	A_s $\text{m}^2 \text{g}^{-1}$	C_s (g L^{-1})	pH_{ZPC}	$\Delta \text{p}K_n^0$	$\log K_{M(\text{OH})_2^+}^0$ tet.	$\log K_{M(\text{OH})_2^+}^0$ mono.	Source of experimental YREE data
α -TiO ₂	Y	-9.0		12.5	14.7	31	5.4	6.3	47.6		Zhang et al. (2004b)
		-9.2							47.6		
α -TiO ₂	Nd	-7.3		12.5	16.9	25	5.4	6.3	49.3		Ridley et al. (2005)
		-7.5							49.3		
Fe ₃ O ₄	Yb	-4.5		6	1.8	12	6.3	5.8	45.6		Marmier et al. (1999b)
Al ₂ O ₃	Yb	-15.0		8	135	2	8.6	5.9	47.3		Marmier et al. (1997)
Al ₂ O ₃	Y ^a	-18.3		8	155	20			47.5		Kosmulski (1997)
Al ₂ O ₃	Gd ^a	-17.5		8	155	20	8.8	5.9	48.3		Kosmulski (1997)
Fe ₂ O ₃	Yb	-19.0		22	8.5	60	8.1	5.5	43.9		Marmier et al. (1997)
Fe ₂ O ₃	La	-16.3	-17.4	22	8.5	2			42.9	22.4	Marmier and Fromage (1999)
		-17.9							42.9	22.4	
		-19.3							42.9	22.4	
		-11.7	-15.9						39.4	20.3	
am-SiO ₂	Yb	-14.7		4.6	384	0.2	2.8	8.4	39.4	20.3	Marmier et al. (1999a)

Values of $\log^* K_{\text{tet.M}(\text{OH})_2^+}^0$ and $\log^* K_{\text{mono.M}(\text{OH})_2^+}^0$ generated by regression of YREE adsorption and surface protonation data refer to the hypothetical 1.0 M standard state and the reactions given below:



Values of $\log K_{\text{tet.M}(\text{OH})_2^+}^0$ and $\log K_{\text{mono.M}(\text{OH})_2^+}^0$ were calculated from the values of $\log^* K_{\text{tet.M}(\text{OH})_2^+}^0$, $\log^* K_{\text{mono.M}(\text{OH})_2^+}^0$, pH_{ZPC} , $\Delta \text{p}K_n^0$, N_s , A_s , and C_s using equations in Appendix A and refer to site-occupancy standard states and the reactions given below:



^a An alternative reaction for Y³⁺ and Gd³⁺ adsorption (dashed curves in Fig. 7) is $4> \text{SOH} + \text{M}^{3+} + \text{H}_2\text{O} = (> \text{SOH})_2 (> \text{SO}^-)_2 \text{M}(\text{OH})_2^{2+} + 3\text{H}^+$ for which values of $\log^* K_{\text{tet.M}(\text{OH})_2^{2+}}^0$ are -12.0 and -11.4, respectively.

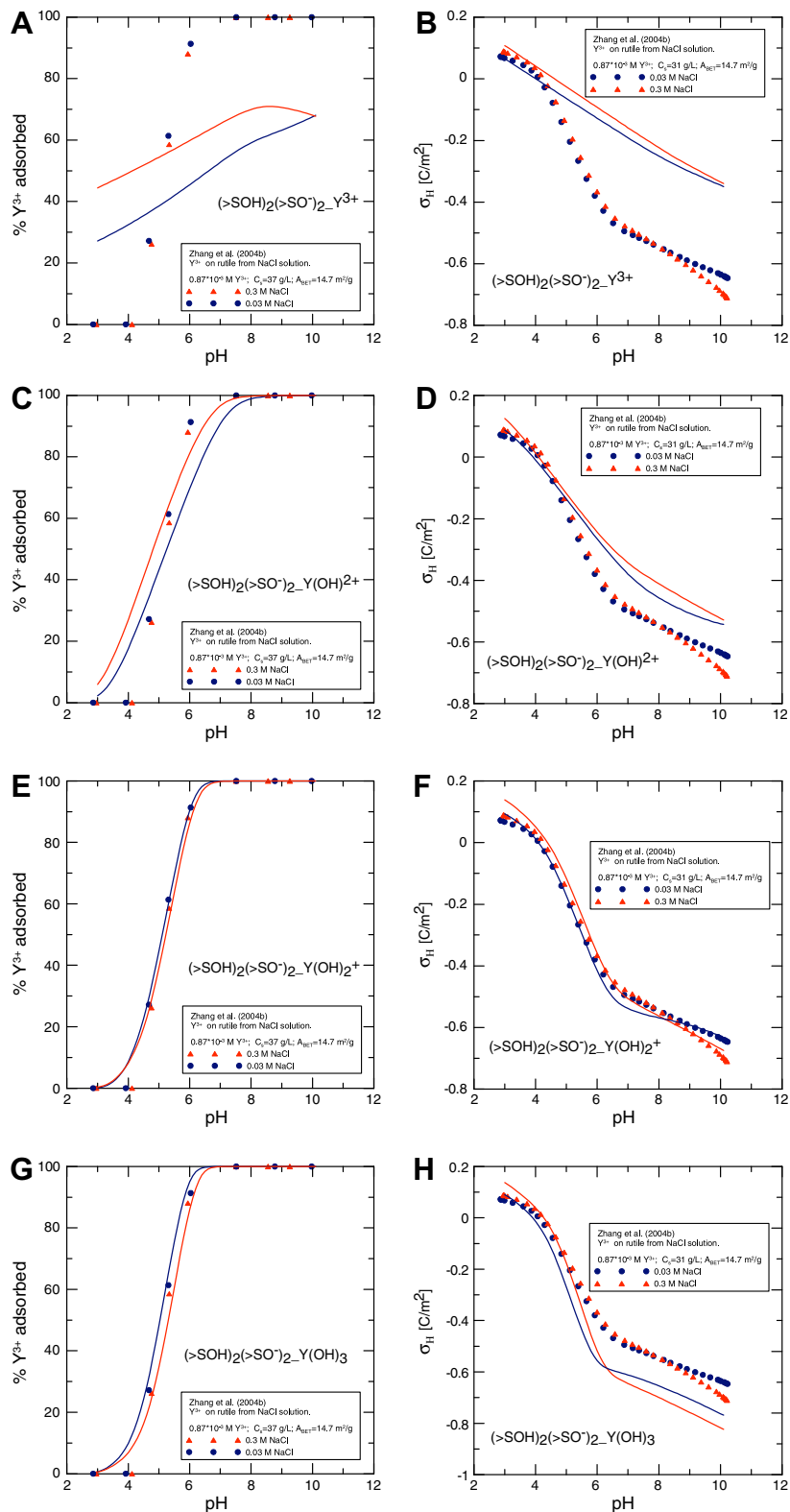


Fig. 2. Proton surface charge in the presence of Y^{3+} and percent Y^{3+} adsorbed on rutile as functions of pH and ionic strength. The symbols represent experimental data (Zhang et al., 2004b). The curves represent regression of the data for four different Y^{3+} model adsorption reactions (Eqs. (1)–(4), see text). Only the reaction producing the dihydroxy surface species $(>SOH)_2(>SO^-)_2-Y(OH)_2^+$ is consistent with both surface protonation and adsorption data.

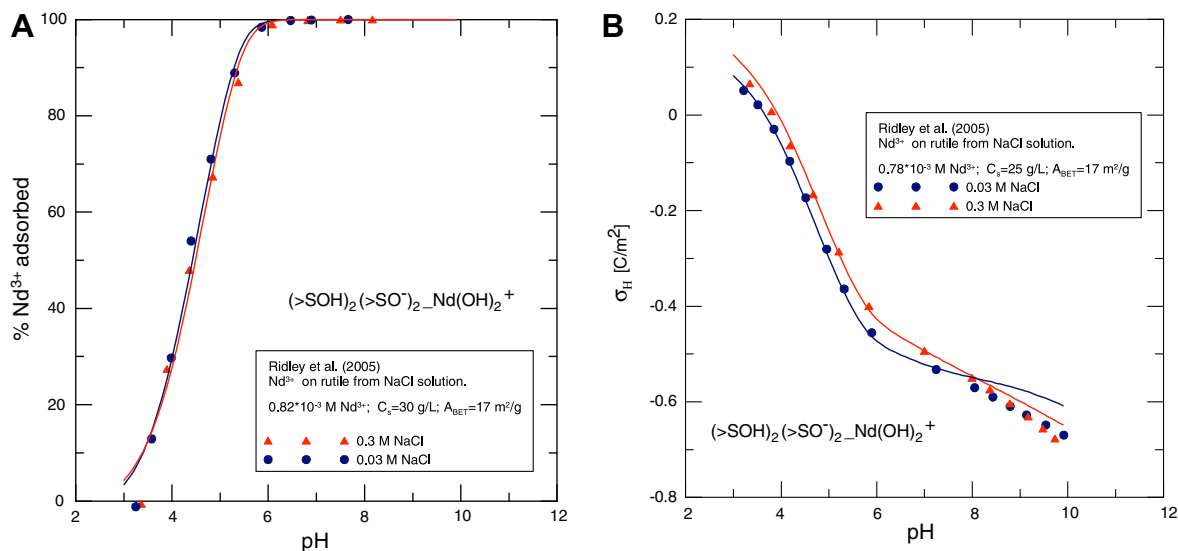


Fig. 3. Proton surface charge in the presence of Nd³⁺ and percent Nd³⁺ adsorbed on rutile as functions of pH and ionic strength. The symbols represent experimental data (Ridley et al., 2005). The curves represent regression of the data using the reaction producing the dihydroxy surface species (Eq. (3)).

YREE, but with two or more surface hydrolysis reactions. For example, in fitting their Nd³⁺/rutile data at 25 C, Ridley et al. (2005) used a combination of MUSIC model analogs of Eqs. (1)–(3). This involved regression for the three corresponding equilibrium constants and an additional electrical capacitance. By so doing, a structurally more complex model than that of the present study was developed, i.e. with four parameters to be determined by regression. Clearly, our current understanding of the state of hydrolysis of Nd³⁺ on rutile depends on the surface complexation model being used. If the hydrolysis state of adsorbed YREE could be experimentally determined, it would help in discriminating between the different surface complexation approaches.

2.3. Yb³⁺ on magnetite, alumina and hematite

Surface protonation data for magnetite and adsorption data for Yb³⁺ on magnetite, alumina and hematite in NaNO₃ solutions at a single surface coverage for each solid (Marmier et al., 1997, 1999b) are represented by the symbols in Fig. 4. The surface protonation data show a normal behavior at pH values above about 6, but below this value the data have an anomalous behavior (cf. the data analyzed in Sverjensky, 2005). The cause of this anomaly is not clear but must be associated with surface reactions in addition to simple proton adsorption. Consequently, only the data referring to pH >6 were regressed to obtain a value for log K_{NO₃⁻}. A value of log K_{Na⁺} was calculated from log K_{NO₃⁻} and pH_{ZPC}.

Two different ionic strengths are represented by the magnetite adsorption data at a surface coverage of 0.92 μmol m⁻² (at 100% coverage). The hematite and alumina data refer to surface coverages of 0.039 and 0.074 μmoles m⁻², respectively, at 100% adsorption. Both adsorption and desorption data were reported for the hematite and alumina and are plotted in Fig. 4 without dis-

tinguishing between them because the results were consistent. However, similar experiments on hematite and alumina at an order of magnitude greater surface coverages (not shown) indicated irreversibility of adsorption, possibly a sign of surface precipitation or surface solid solution uptake of Yb³⁺ similar to Lu³⁺ (Marmier et al., 1997; Dardenne et al., 2002). As a consequence, even though the experiments analyzed here for Yb³⁺ on hematite and alumina involved consistent adsorption and desorption results, our analysis should be regarded as a first approximation only.

The solid curves in the figures represent regression of the experimental data. All three datasets for Yb³⁺ adsorption are again noteworthy for the steep adsorption edges at pH values less than the pH_{ZPC}. The scatter in the large number of datapoints suggests that the overall experimental uncertainty in the percent adsorbed may be of the order of ±5–10. It can be seen in Fig. 4 that the model curves representing the dihydroxy Yb³⁺ complex (i.e. Eq. (3)) are consistent with much of the experimental data within this uncertainty, with the exception of some of the data at about 50% adsorption. Furthermore, it can be seen in Fig. 4b that the model predicts a negligible dependence of the adsorption on ionic strength, which is consistent with the lack of ionic strength dependence of the experimental data.

2.4. Yb³⁺ on silica

Adsorption data for Yb³⁺ on silica in NaNO₃ solutions at two ionic strengths and two surface coverages (Marmier et al., 1999a) are represented by the symbols in Fig. 5A and B. The data in Fig. 5A represent a relatively low surface coverage of 0.026 μmol m⁻² at 100% adsorption, whereas the data in Fig. 5B represent a higher surface coverage of 0.26 μmol m⁻² at 100% adsorption. Two different ionic strengths are represented in the lower surface coverage

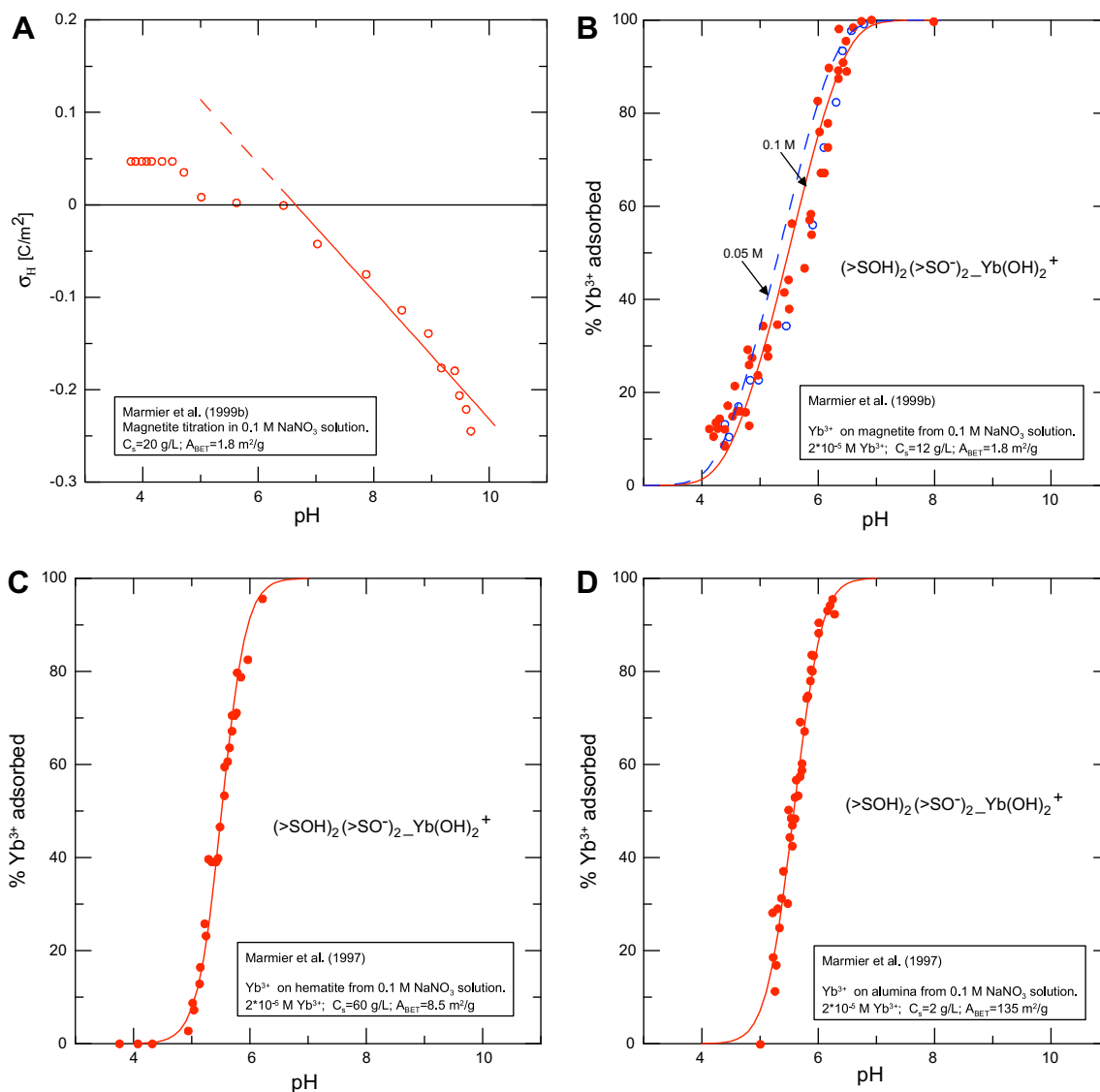
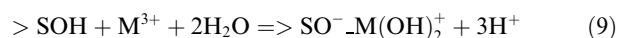


Fig. 4. Proton surface charge for magnetite in $NaNO_3$ solutions and percent Yb^{3+} adsorbed on magnetite, hematite and alumina as functions of pH and ionic strength. The symbols represent experimental data (Marmier et al., 1997, 1999b), open symbols represent 0.05 M and closed symbols represent 0.1 M $NaNO_3$. The curves represent regression of the data using the reaction producing the dihydroxy surface species (Eq. (3)).

data. No results on the reversability of adsorption were reported. In Fig. 5A and B, the curves again represent regression of the data with the dihydroxy tetranuclear surface complex of Yb^{3+} . However, the same experimental data are shown in Fig. 5C and D, where the curves represent regression with dihydroxy tetranuclear and mononuclear surface complexes of Yb^{3+} . It can be seen in Fig. 5A and B that although the dihydroxy Yb^{3+} complex alone (i.e. Eq. (3)) can account for the low surface coverage data at the two ionic strengths, it cannot account for the experimental data at the higher surface coverage. Possible explanations for this include surface precipitation or a change in the surface speciation of adsorbed Yb^{3+} (i.e. a second surface species). The simplest surface precipitate would be $Yb(OH)_3$, which happens to be one of the most insoluble of the YREE hydroxides (Baes and Mesmer, 1976). For

the total Yb^{3+} concentration in the experiments of Fig. 5, the pH for precipitation of $Yb(OH)_3$ is about 6.5. It can be seen in Fig. 5A that the bulk of the adsorption has taken place by this pH. However, in Fig. 5B, it can be seen that most of the adsorption is apparently taking place at pH values greater than 6.5. Consequently, it is possible that most of the data in Fig. 5B refer to surface precipitation rather than adsorption. This could account for the discrepancy between the data and the calculated adsorption curve.

We also investigated the possibility that the discrepancy in Fig. 5B can be attributed to the formation of a second surface species. Regression calculations indicated that a dihydroxy complex coordinated to one surface site with the reaction stoichiometry



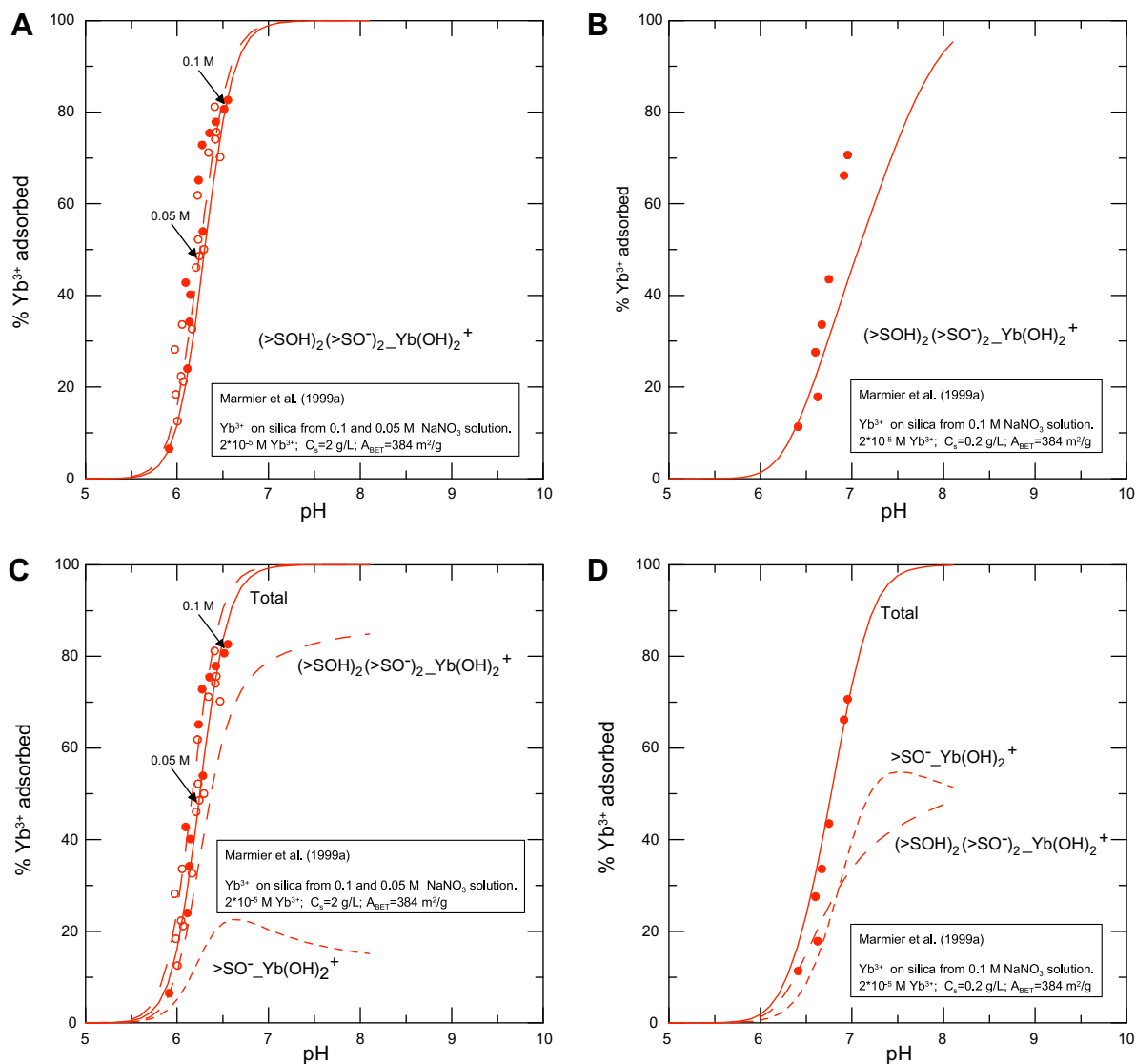


Fig. 5. Yb^{3+} adsorbed on silica in NaNO_3 solutions as a function of pH, ionic strength and surface coverage. The symbols represent experimental data (Marmier et al., 1999a), open symbols represent 0.05 M and closed symbols represent 0.1 M NaNO_3 . The curves in Fig. 5A and B represent regression of the data using the reaction producing the dihydroxy surface species (Eq. (3)). The solid curves in Fig. 5C and D were generated using two reactions for the adsorbed Yb^{3+} (Eqs. (3) and (9)). The dashed curves in these figures refer to the individual surface species contributions in 0.1 M NaNO_3 solutions (see text for details).

together with the tetra-complex was consistent with the experimental data (Fig. 5C and D). The equilibrium constant corresponding to Eq. (9) is given by

$$\log^* K^{\theta}_{\text{mono-M}(\text{OH})_2^+} = \frac{a_{>\text{SO}^- \text{M}(\text{OH})_2^+} a_{\text{H}^+}^3}{a_{>\text{SOH}} a_{\text{M}^{3+}} a_{\text{H}_2\text{O}}^2} 10^{\frac{F(\psi_{\beta} - \psi_0)}{2.303RT}} \quad (10)$$

It can be seen in Fig. 5B and C that the importance of the mononuclear complex increases from about 20% to about 40% of the total adsorption with increasing surface coverage. This result is closely analogous to what was previously found for the surface speciation of the alkaline earths (Sverjensky, 2006). Adsorption data for the alkaline earths referring to a wide range of surface coverages required at least two surface species, one tetra- and one

mononuclear, particularly for the smaller alkaline earths Mg^{2+} and Ca^{2+} . Molecular dynamics calculations for alkaline earth adsorption on rutile also indicate more than one surface species on rutile (Predota et al., 2004a,b). Distinguishing between the formation of a surface precipitate and an additional surface adsorbed species will require further experimental studies.

2.5. La^{3+} on hematite

Surface protonation and adsorption data for La^{3+} on hematite in NaNO_3 solutions at three surface coverages (Marmier and Fromage, 1999) are represented by the symbols in Fig. 6A–D. The lower surface coverage (Fig. 6B) is $0.039 \mu\text{mol m}^{-2}$, the highest surface coverage (Fig. 6D) is

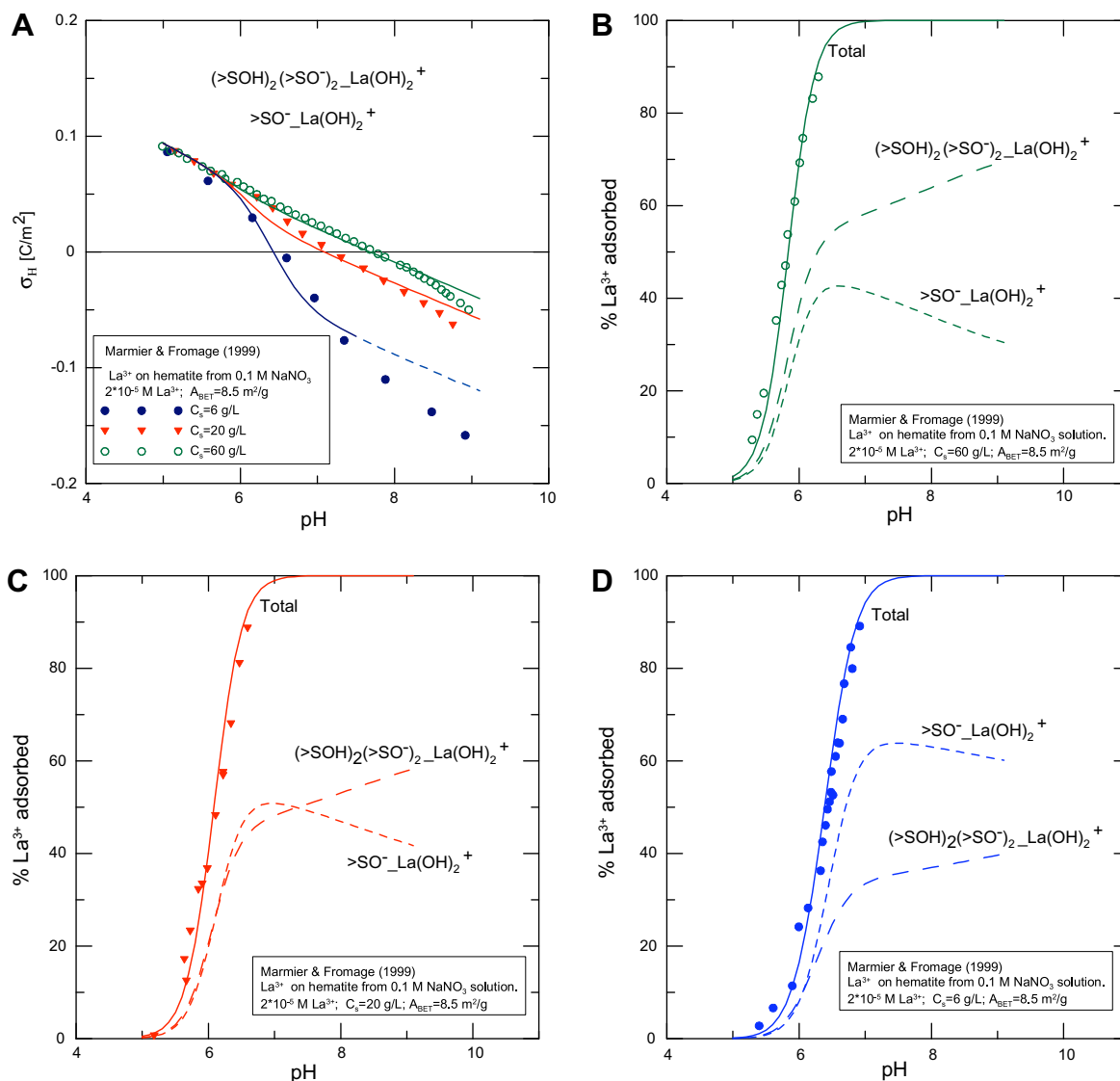


Fig. 6. Proton surface charge in the presence of La³⁺ and percent La³⁺ adsorbed on hematite as functions of pH and surface coverage. The symbols represent experimental data (Marmier and Fromage, 1999). The solid curves represent regression of the data using the reactions producing the tetranuclear dihydroxy surface species (Eq. (3)) and the mononuclear dihydroxy surface species (Eq. (9)). The dashed curves in Fig. 6B–D represent the individual contributions of the two surface species.

$0.39 \mu\text{mol m}^{-2}$ at 100% adsorption. Experiments representing different equilibration times from 1 to 21 h were all consistent. However, no results on the reversibility of adsorption were reported.

The solid curves in Fig. 6 represent regression calculations. As with Yb³⁺ on silica (Fig. 5), the tetranuclear species alone was not sufficient to fit the data in Fig. 6 as a function of surface coverage. However, precipitation of La(OH)₃ seems unlikely under the conditions of the adsorption experiments in Fig. 6B–D because La(OH)₃ is much more soluble than Yb(OH)₃ (Baes and Mesmer, 1976). For the total La³⁺ concentration in these experiments, the pH for precipitation of La(OH)₃ is about 8.4. Consequently, as a first approximation we used the two reactions established above (Eqs. (3) and (9)) to describe the adsorption data in Fig. 6B–D, within $\pm 5\%$ adsorbed. The calculated surface speciation for the different

surface coverages show a clear trend of increasing relative importance of the mono- versus the tetranuclear dihydroxy surface species as surface coverage increases.

The calculated curves for surface protonation in Fig. 6A, however, show an increasing discrepancy with the data above pH 7 at the highest surface coverage and above pH 8 at the lower surface coverages. Repeated efforts to obtain a better fit to the data using surface species with different hydrolysis states failed to satisfactorily fit both the adsorption and surface protonation data over the whole range of conditions in Fig. 6A–D. Given the evidence for irreversible adsorption discussed above for Yb³⁺ on hematite at surface coverages of greater than $0.39 \mu\text{mol m}^{-2}$, these results suggest that perhaps surface precipitation or surface solid solution uptake is occurring at pH values greater than about 7.0 for La³⁺ on hematite. Based on the discussion above, it

seems unlikely that a surface precipitate of $\text{La}(\text{OH})_3$ is forming. A surface solid solution may be more likely in this instance, as uptake of Lu^{3+} during aging of ferrihydrite has been documented experimentally (Dardenne et al., 2002).

2.6. Gd^{3+} and Y^{3+} on alumina

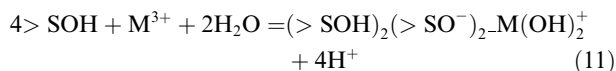
Adsorption data for Gd^{3+} and Y^{3+} on alumina in NaClO_4 solutions at a single surface coverage (Kosmulski, 1997) are represented by the symbols in Fig. 7. The surface coverage, which is 0.16 nmol m^{-2} at 100% adsorption, is much lower than any other analyzed in the present study. Experiments representing different temperatures from 15 to 35 °C are plotted.

The curves in Fig. 7 represent regression calculations referring to 25 °C for two different reaction stoichiometries involving tetranuclear species. The reaction involving the dihydroxy species used throughout this study (Eq. (3)) fits the 25 °C Gd^{3+} data within ± 5 –10% adsorbed. However, the monohydroxy species (Eq. (2)) also fits the 25 °C data within ± 5 –10% adsorbed. As a first approximation, the same conclusion could be drawn for the Y^{3+} curves in Fig. 7 where only data referring to 15 and 35 °C are available. These results are in contrast to the adsorption (and surface protonation) data for Y^{3+} on rutile in Fig. 2, where Eq. (2) is clearly inadequate as the major reaction. However, the calculations in Fig. 2 do not rule out the reaction in Eq. (2) as a minor species under the conditions of the experiments being considered.

3. SUMMARY AND CONCLUDING REMARKS ON THE SURFACE SPECIATION OF YREE ON OXIDES

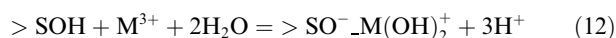
The regression calculations discussed above indicate that the tetranuclear Y^{3+} surface species established by X-ray studies for the rutile (110) surface is applicable to adsorp-

tion studies of YREE on other oxides. Over wide ranges of pH and ionic strength, the reaction producing a hydrolyzed tetranuclear surface species



accounted for a significant fraction of the adsorbed YREE on rutile, hematite, alumina and silica. Because these oxides cover the entire spectrum of adsorption behavior for protons and electrolytes (Sverjensky, 2005, 2006), it can be expected that Eq. (11) will apply to all oxides, assuming that a tetrahedral site exists.

Where adsorption data were available as a function of surface coverage for hematite and silica, an additional reaction stoichiometry could be used at the higher surface coverages. Regression calculations indicated a hydrolyzed mononuclear surface species consistent with the reaction



Although a mononuclear surface species of Y^{3+} was not detected in the X-ray studies of the rutile (110) surface, nor was it needed to describe Y^{3+} or Nd^{3+} adsorption and surface protonation data on rutile (Figs. 2 and 3), the proportions of tetra- and mononuclear surface species can be expected to vary as functions of pH, ionic strength, surface coverage, and type of oxide. We therefore infer that a mono-complex would be weaker (relative to the tetra-complex) on rutile compared with hematite or silica. A possible explanation for this could involve differences in the solvation environment for these different solids. According to Born solvation theory, high dielectric constant solids such as rutile can have a different proportion of surface species compared to lower dielectric constant solids (cf. alkaline earths, Sverjensky, 2006; arsenate, Fukushi and Sverjensky, 2007a).

An alternative to the use of Eq. (12) at the highest surface coverages and pH values analyzed here, particularly

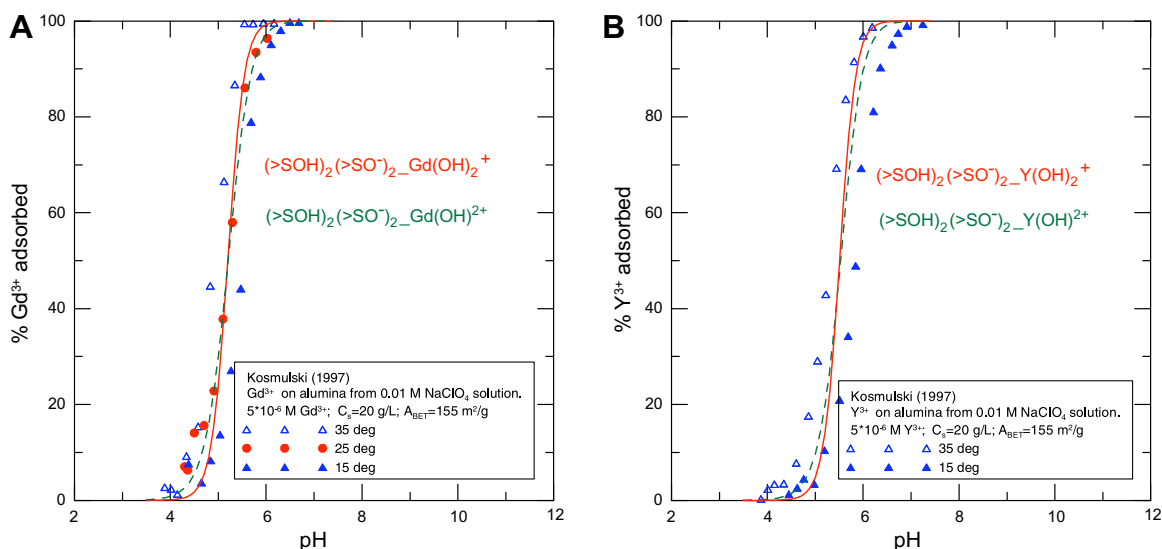


Fig. 7. Gd^{3+} and Y^{3+} adsorbed on alumina in NaClO_4 solutions as a function of pH and temperature. The symbols represent experimental data (taken from Figs. 3 and 7 of Kosmulski, 1997). The solid curves represent regression of the data using the reaction producing the dihydroxy surface species (Eq. (3)). The dashed curves represent regression of the data using the reaction producing the monohydroxy surface species (Eq. (2)).

for Yb^{3+} on silica, could be precipitation of $\text{Yb}(\text{OH})_3$. Similarly, surface protonation data for La^{3+} on hematite at the higher surface coverages, as well as experimental data for the irreversibility of adsorption of Yb^{3+} on hematite, suggest that surface precipitation or surface solid solution uptake of YREE might be occurring. Indications of solid solution formation involving YREE and iron oxides were reported for La^{3+} with aged ferrihydrite (Dardenne et al., 2002). Additional experimental adsorption data and X-ray studies of YREE as functions of surface coverage are needed to test this hypothesis.

The reactions used in the present study apply specifically to the ETLM of surface complexation. It is interesting that only a single hydrolysis state is indicated. In contrast, other surface complexation approaches required more complex speciation schemes involving two to four reactions differing in the hydrolysis state of the adsorbed metal (e.g. Marmier et al., 1997, 1999a; Ridley et al., 2005). Clearly, experimental methods that can establish the state of hydrolysis of adsorbed YREE on oxides would be extremely valuable in constraining the surface complexation approaches.

It can also be expected that under some conditions, additional surface complexes of YREE will become important. For example, experimental data and model calculations for the scavenging of YREE by precipitating HFO indicate the need for ternary complexes of YREE with carbonate on HFO (Quinn et al., 2006b). The results of the present study provide an internally consistent basis which could be used to investigate such systems. For example, the present study has established YREE adsorption reactions consistent with a wide variety of oxides under carbonate-free conditions. Independent calibration of the ETLM for carbonate adsorption in the absence of YREE will enable prediction of the effect of carbonate involved in aqueous and surface complexation. In YREE-bearing systems, the effects of ternary YREE-carbonate surface complexes could then be evaluated while simultaneously taking account of carbonate aqueous and surface complexation in competition with electrolyte species. This approach could also be used to investigate the presence and complexing behavior of other ligands expected to influence the surface chemical behavior of YREE, for example organic ligands (Davranche et al., 2004, 2005).

ACKNOWLEDGMENTS

The authors greatly appreciate discussions with and data provided by M. Machesky and M. Ridley. We also benefitted from discussions with P. Fenter, K. Fukushi, and D. Wesolowski. Financial support to W. Piasecki was provided by a scholarship from the Foundation for Polish Science. Financial support to D. A. Sverjensky was provided by DOE Grant DE-FG02-96ER-14616 and DuPont.

APPENDIX

Many studies still make use of the hypothetical 1.0 M standard state for surface species. However, equilibrium constants on this basis include a dependence on site density, surface area, and in some instances, solid concentration (Sverjensky, 2003). Such equilibrium constants for different

samples of the same solid, or different solids, cannot be sensibly compared. In order to be able to compare, correlate and predict equilibrium constants for surface species, it is essential to use an internally consistent set of surface protonation, electrolyte adsorption, and metal adsorption equilibrium constants referring to standard states independent of site densities, surface areas and solid concentrations. The site-occupancy standard states described below were developed for this purpose. Equations for the conversion from the hypothetical 1.0 M standard state to the site-occupancy standard states are also summarized below.

Equilibrium constants in the present study written with the superscript “ θ ”, e.g. K^θ , refer to site-occupancy standard states (Sverjensky, 2003). They can be summarized as follows. The standard state for sorbent sites ($>\text{SOH}$) refers to unit activity of surface sorption sites on a completely unsaturated surface at any P and T such that

$$a_{>\text{SOH}} = \lambda_{>\text{SOH}} X_{>\text{SOH}} \quad (\text{A1})$$

and $\lambda_{>\text{SOH}} \rightarrow 1$ as $X_{>\text{SOH}} \rightarrow 1$. In these relations, $a_{>\text{SOH}}$, $\lambda_{>\text{SOH}}$ and $X_{>\text{SOH}}$ represent the activity, activity coefficient and mole fraction of $>\text{SOH}$ sites, respectively. This is, in principle, a physically achievable standard state. For any sorbate species ($>j$), the standard state refers to unit activity of surface species on a completely saturated surface with zero potential at any P and T referenced to infinite dilution, expressed by

$$a_{>j} = \lambda_{>j} X_{>j} \quad (\text{A2})$$

where $\lambda_{>j} \rightarrow 1$ and the electrochemical surface potential approaches zero as $X_{>j} \rightarrow 0$. As above, $a_{>j}$, $\lambda_{>j}$ and $X_{>j}$ represent the activity, activity coefficient and mole fraction of the $>j$ th sorbate species, respectively. This is a hypothetical standard state, i.e. not physically achievable.

An advantage of defining the standard states for sorbent sites and sorbate species in this way is that in model calculations the limiting conditions of $X_{>\text{SOH}} \rightarrow 1$ and $X_{>j} \rightarrow 0$ are often approached. In other words, for the triple-layer model used here, $>\text{SOH}$ is commonly by far the dominant species, whereas sorbates such as $>\text{SOH}_2^+$, $>\text{SOH}_2^+ \cdot \text{NO}_3^-$ and $>(\text{SOH})_2 (>\text{SO}^-)_2 \cdot \text{M}(\text{OH})_2^+$ are often minor species. Under these circumstances, it is reasonable to assume that $\lambda_{>\text{SOH}} \approx 1$ and $\lambda_{>j} \approx 1$.

For the surface protonation reactions



the standard states adopted above are related to the widely used hypothetical 1.0 M standard state (written with a superscript “0”, Sverjensky, 2003) by

$$\log K_1^\theta = \log K_1^0 + \log \left(\frac{N_s A_s}{N^i A^i} \right) \quad (\text{A7})$$

$$\log K_2^\theta = \log K_2^0 - \log \left(\frac{N_s A_s}{N^i A^i} \right) \quad (\text{A8})$$

$$\log K_{\text{ZPC}}^\theta = \log K_{\text{ZPC}}^0 \quad (\text{A9})$$

and

$$\log K_n^\theta = \log K_n^0 - 2 \log \left(\frac{N_s A_s}{N^\ddagger A^\ddagger} \right) \quad (\text{A10})$$

respectively, where

N_s represents the surface site density on the sth solid sorbent (sites m^{-2})

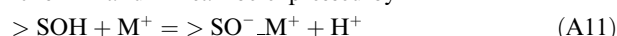
N^\ddagger represents the standard state sorbate species site density (sites m^{-2})

A_s represents the BET surface area of the sth solid sorbent ($\text{m}^2 \text{g}^{-1}$)

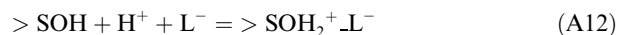
A^\ddagger represents a standard state BET surface area ($\text{m}^2 \text{g}^{-1}$)

In the present study, values of $N^\ddagger = 10 \times 10^{18}$ sites m^{-2} and $A^\ddagger = 10 \text{ m}^2 \text{g}^{-1}$ are selected for all solids. It is emphasized that these values are properties of the hypothetical site-occupancy standard state for sorbate species applicable to all samples of all solids.

Equilibria for adsorption of the monovalent electrolyte ions M^+ and L^- can be expressed by



and



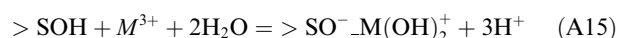
for which

$$\log^* K_{M^+}^\theta = \log^* K_{M^+}^0 + \log \left(\frac{N_s A_s}{N^\ddagger A^\ddagger} \right) \quad (\text{A13})$$

and

$$\log^* K_{L^-}^\theta = \log^* K_{L^-}^0 + \log \left(\frac{N_s A_s}{N^\ddagger A^\ddagger} \right) \quad (\text{A14})$$

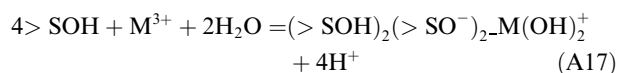
Equilibria for adsorption of trivalent YREE cations used in the present study can be expressed by



where

$$\log^* K_{>\text{SO}^- \text{M}(\text{OH})_2^+}^\theta = \log \left(\frac{a_{>\text{SO}^- \text{M}(\text{OH})_2^+} a_{\text{H}^+}^3}{a_{>\text{SOH}} a_{M^{3+}} a_{\text{H}_2\text{O}}^2} \right) + \frac{F(\psi_\beta - \psi_0)}{2.303RT} \quad (\text{A16})$$

and



where

$$\log^* K_{\text{tet.M}(\text{OH})_2^+}^\theta = \log \left(\frac{a_{(>\text{SOH})_2 (>\text{SO}^-)_2 \text{M}(\text{OH})_2^+} a_{\text{H}^+}^4}{a_{>\text{SOH}}^2 a_{M^{3+}}^2 a_{\text{H}_2\text{O}}^2} \right) + \frac{F(\psi_\beta - 2\psi_0)}{2.303RT} \quad (\text{A18})$$

For these reactions, the relationship to the hypothetical 1.0 M standard state is given by

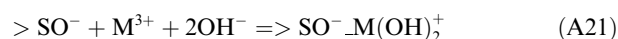
$$\log^* K_{>\text{SO}^- \text{M}(\text{OH})^+}^\theta = \log^* K_{>\text{SO}^- \text{M}(\text{OH})^+}^0 + \log \left(\frac{N_s A_s}{N^\ddagger A^\ddagger} \right) \quad (\text{A19})$$

and

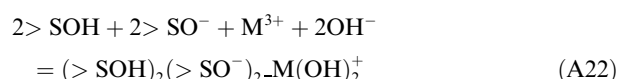
$$\log^* K_{\text{tet.M}(\text{OH})_2^+}^\theta = \log^* K_{\text{tet.M}(\text{OH})_2^+}^0 + \log \left(\frac{(N_s A_s)^4}{N^\ddagger A^\ddagger} C_s^3 \right) \quad (\text{A20})$$

In Eq. (A20), the dependence on site density and surface area to the 4th power is a result of the coefficient of 4 $>\text{SOH}$ in reaction (A17). The dependence on solid concentration (C_s) is expressed to the 3rd power because the sorbate dependence is assumed to cancel with the sorbent. This reduces the dependence for solid concentration from the 4th power to the 3rd power.

Finally, the reactions in Eqs. (A15) and (A17) can also be expressed for comparative purposes relative to the charged sites $>\text{SO}^-$ and aqueous OH^- as



and



for which the equilibrium constants can be calculated with

$$\log K_{>\text{SO}^- \text{M}(\text{OH})^+}^\theta = \log^* K_{>\text{SO}^- \text{M}(\text{OH})^+}^\theta + p\text{H}_{\text{ZPC}} + \frac{\Delta p K_n^\theta}{2} + 28.0 \quad (\text{A23})$$

and

$$\log K_{\text{tet.M}(\text{OH})_2^+}^\theta = \log^* K_{\text{tet.M}(\text{OH})_2^+}^\theta + 2p\text{H}_{\text{ZPC}} + \Delta p K_n^\theta + 28.0 \quad (\text{A24})$$

In these equations, the value of 28.0 represents $2 \log K_{\text{H}_2\text{O}}$. The values of $\log K_{>\text{SO}^- \text{M}(\text{OH})^+}^\theta$ and $\log K_{\text{tet.M}(\text{OH})_2^+}^\theta$ given in Table 2 of the present study were calculated from the values of $\log^* K_{>\text{SO}^- \text{M}(\text{OH})^+}^\theta$ and $\log^* K_{\text{tet.M}(\text{OH})_2^+}^\theta$ in Table 2 using Eqs. (A19), (A20) and (A23), and (A24).

REFERENCES

- Baes C. F. and Mesmer R. E. (1976) *The Hydrolysis of Cations*. John Wiley and Sons, Inc., New York.
- Bau M. (1999) Scavenging of dissolved yttrium and rare earths by precipitating iron oxyhydroxide: experimental evidence for Ce oxidation, Y-Ho fractionation, and lanthanide tetrad effect. *Geochim. Cosmochim. Acta* **63**, 67–77.
- Bau M., Alexander B., Chesley J. T., Dulski P. and Brantley S. L. (2004) Mineral dissolution in the Cape Cod aquifer, Massachusetts, USA. I. Reaction stoichiometry and impact of accessory feldspar and glauconite on strontium isotopes, solute concentrations, and REY distribution. *Geochim. Cosmochim. Acta* **68**, 1199–1216.
- Byrne R. H. (2002) Inorganic speciation of dissolved elements in seawater: the influence of pH on concentration ratios. *Geochem. Trans.* **3**, 11–16.
- Byrne R. H. and Kim K. (1990) Rare earth element scavenging in seawater. *Geochim. Cosmochim. Acta* **54**, 2645–2656.
- Coppin F., Berger G., Bauer A., Castet S. and Loubet M. (2002) Sorption of lanthanides on smectite and kaolinite. *Chem. Geol.* **182**, 57–68.
- Dardenne K., Schafer T., Denecke M. A., Rothe J. and Kim J. I. (2001) Identification and characterization of sorbed lutetium

- species on 2-line ferrihydrite by sorption data modeling, TRLS and EXAFS. *Radiochim. Acta* **89**, 469–479.
- Dardenne K., Schafer T., Lindqvist-Reis P., Denecke M. A., Plaschke M., Rothe J. and Kim J. I. (2002) Low temperature XAFS investigation of the lutetium binding changes during the 2-line ferrihydrite alteration process. *Environ. Sci. Technol.* **36**, 5092–5099.
- Davranche M., Pourret O., Gruau G. and Dia A. (2004) Impact of humate complexation on the adsorption of REE onto Fe oxyhydroxide. *J. Colloid Interf. Sci.* **277**, 271–279.
- Davranche M., Pourret O., Gruau G., Dia A. and Le Coz-Bouhnik M. (2005) Adsorption of REE(III)–humate complexes onto MnO₂: experimental evidence for Ce anomaly and lanthanide tetrad effect suppression. *Geochim. Cosmochim. Acta* **69**, 4825–4835.
- De Carlo E. H., Wen X. and Irving M. (1998) The influence of redox reactions on the uptake of dissolved Ce by suspended Fe and Mn oxide particles. *Aquat. Geochem.* **3**, 357–389.
- Farley K. J., Dzombak D. A. and Morel F. M. M. (1985) A surface precipitation model for the sorption of cations on metal oxides. *J. Colloid Interf. Sci.* **106**, 226–242.
- Fukushi K. and Sverjensky D. A. (2007a) A predictive model for arsenate adsorption and surface speciation on oxides consistent with spectroscopic and theoretical molecular evidence. *Geochim. Cosmochim. Acta* **71**, 3717–3745.
- Fukushi K. and Sverjensky D. A. (2007b) A surface complexation model for sulfate and selenate on iron oxides consistent with spectroscopic and theoretical molecular evidence. *Geochim. Cosmochim. Acta* **71**, 1–24.
- Gammons C. H., Wood S. A. and Nimick D. A. (2005) Diel behavior of rare earth elements in a mountain stream with acidic to neutral pH. *Geochim. Cosmochim. Acta* **69**, 3747–3758.
- Haley B. A., Klinkhammer G. P. and McManus J. (2004) Rare earth elements in pore waters of marine sediments. *Geochim. Cosmochim. Acta* **68**, 1265–1279.
- Johannesson K. H., Hawkins, Jr., D. L. and Cortés A. (2006) Do Archean chemical sediments record ancient seawater rare earth element patterns? *Geochim. Cosmochim. Acta* **70**, 871–890.
- Katz L. E. and Hayes K. F. (1995) Surface complexation modeling. II. Strategy for modeling polymer and precipitation reactions at high surface coverage. *J. Colloid Interf. Sci.* **170**, 491–501.
- Klungness G. D. and Byrne R. H. (2000) Comparative hydrolysis behavior of the rare earths and yttrium: the influence of temperature and ionic strength. *Polyhedron* **19**, 99–107.
- Koepfenkastro D. and De Carlo E. H. (1992) Sorption of rare-earth elements from seawater onto synthetic mineral particles: an experimental approach. *Chem. Geol.* **95**, 251–263.
- Koschinsky A. and Hein J. R. (2003) Uptake of elements from seawater by ferromanganese crusts: solid-phase associations and seawater speciation. *Mar. Geol.* **198**, 331–351.
- Kosmulski M. (1997) Standard enthalpies of adsorption of di- and trivalent cations on alumina. *J. Colloid Interf. Sci.* **192**, 215–227.
- Kowal-Fouchard A., Drot R., Simoni E., Marmier N., Fromage F. and Ehrhardt J. (2004) Structural identification of europium(III) adsorption complexes on montmorillonite. *New J. Chem.* **28**, 864–869.
- Luo Y. R. and Byrne R. H. (2001) Yttrium and rare earth element complexation by chloride ions at 25 degrees C. *J. Solution Chem.* **30**, 837–845.
- Marmier N. and Fromage F. (1999) Comparing electrostatic and non-electrostatic surface complexation modeling of the sorption of lanthanum on hematite. *J. Colloid Interf. Sci.* **212**, 252–263.
- Marmier N., Dumonceau A. J. and Fromage F. (1997) Surface complexation modeling of Yb(III) sorption and desorption on hematite and alumina. *J. Contam. Hydrol.* **26**, 159–167.
- Marmier N., Delisée J. A. and Fromage F. (1999a) Surface complexation modeling of Yb(III) and Cs(I) sorption on silica. *J. Colloid Interf. Sci.* **212**, 228–233.
- Marmier N., Delisée A. and Fromage F. (1999b) Surface complexation modeling of Yb(III), Ni(II), and Cs(I) sorption on magnetite. *J. Colloid Interf. Sci.* **211**, 54–60.
- Music S. and Ristic R. (1988) Adsorption of trace elements or radionuclides on hydrous oxides. *J. Radioanal. Nucl. Chem.* **120**, 289–304.
- Ohta A. and Kawabe I. (2000) Theoretical study of tetrad effects observed in REE distribution coefficients between marine Fe–Mn deposit and deep seawater, and in REE(III)–carbonate complexation constants. *Geochem. J.* **34**, 455–473.
- Ohta A. and Kawabe I. (2001) REE(III) adsorption onto Mn dioxide (δ -MnO₂) and Fe oxyhydroxide: Ce(III) oxidation by δ -MnO₂. *Geochim. Cosmochim. Acta* **65**, 695–703.
- Predota M., Bandura A. V., Cummings P. T., Kubicki J. D., Wesolowski D. J., Chialvo A. A. and Machesky M. (2004a) Electric double layer at the rutile (110) surface. 1. Structure of surfaces and interfacial water from molecular dynamics by use of ab initio potentials. *J. Phys. Chem. B* **108**, 12049–12060.
- Predota M., Zhang Z., Fenter P., Wesolowski D. J. and Cummings P. T. (2004b) Electric double layer at the rutile (110) surface. 2. Adsorption of ions from molecular dynamics and X-ray experiments. *J. Phys. Chem. B* **108**, 12061–12072.
- Quinn K. A., Byrne R. H. and Schijf J. (2004) Comparative scavenging of yttrium and the rare earth elements in seawater: competitive influences of solution and surface chemistry. *Aquat. Geochem.* **10**, 59–80.
- Quinn K. A., Byrne R. H. and Schijf J. (2006a) Sorption of yttrium and rare earth elements by amorphous ferric hydroxide: influence of pH and ionic strength. *Mar. Chem.* **99**, 128–150.
- Quinn K. A., Byrne R. H. and Schijf J. (2006b) Sorption of yttrium and rare earth elements by amorphous ferric hydroxide: influence of solution complexation with carbonate. *Geochim. Cosmochim. Acta* **70**, 4151–4165.
- Quinn K. A., Byrne R. H. and Schijf J. (2007) Sorption of yttrium and rare earth elements by amorphous ferric hydroxide: influence of temperature. *Environ. Sci. Technol.* **41**, 541–546.
- Rabung T., Geckeis H., Kim J. and Beck H. P. (1998) Sorption of Eu(III) on a natural hematite: application of a surface complexation model. *J. Colloid Interf. Sci.* **208**, 153–161.
- Ragnarsdottir K. V., Oelkers E. H., Sherman D. M. and Collins C. M. (1998) Aqueous speciation of yttrium at temperatures from 25 to 340 degrees C at P-sat: an in situ EXAFS study. *Chem. Geol.* **151**, 29–39.
- Ridley M. K., Machesky M. L., Wesolowski D. J. and Palmer D. A. (2005) Surface complexation of neodymium at the rutile–water interface: a potentiometric and modeling study in NaCl media to 250 °C. *Geochim. Cosmochim. Acta* **69**, 63–81.
- Rizkalla E. N. and Choppin G. R. (1991) Hydration and hydrolysis of lanthanides. In *Handbook on the physics Chemistry of rare earths Rare Earths* (eds. K. A. Gschneidner, Jr. and L. Eyring). Elsevier, Amsterdam.
- Schindler P. W. and Stumm W. (1987) The surface chemistry of oxides, hydroxides, and oxide minerals. In *Aquatic Surface Chemistry: Chemical Processes at the Particle–Water Particle–Water Interface* (ed. W. Stumm). John Wiley and Sons, New York.
- Sholkovitz E. R. (1992) Chemical evolution of rare earth elements: fractionation between colloidal and solution phases of filtered river water. *Earth Planet. Sci. Lett.* **114**, 77–84.
- Smyth J. R. and Bish D. L. (1988) *Crystal Structures and Cation Sites of the Rock-Forming Minerals*. Allen and Unwin, Boston.
- Sverjensky D. A. (2001) Interpretation and prediction of triple-layer model capacitances and the structure of the oxide–

- electrolyte–water interface. *Geochim. Cosmochim. Acta* **65**, 3643–3655.
- Sverjensky D. A. (2003) Standard states for the activities of mineral surface-sites and species. *Geochim. Cosmochim. Acta* **67**, 17–28.
- Sverjensky D. A. (2005) Prediction of surface charge on oxides in salt solutions: revisions for 1:1 (M^+L^-) electrolytes. *Geochim. Cosmochim. Acta* **69**, 225–257.
- Sverjensky D. A. (2006) Prediction of the speciation of alkaline earths adsorbed on mineral surfaces in salt solutions. *Geochim. Cosmochim. Acta* **70**, 2427–2453.
- Sverjensky D. A. and Fukushi K. (2006) A predictive model (ETLM) for As(III) adsorption and surface speciation on oxides consistent with spectroscopic data. *Geochim. Cosmochim. Acta* **70**, 3778–3802.
- Tang J. and Johannesson K. H. (2005) Adsorption of rare earth elements onto Carrizo sand: experimental investigations and modeling with surface complexation. *Geochim. Cosmochim. Acta* **69**, 5247–5261.
- Tao Z., Wang X., Guo Z. and Chu T. (2004) Is there a tetrad effect in the adsorption of lanthanides (III) at solid–water interfaces? *Colloids Surf. A* **251**, 19–25.
- Verplanck P. L., Nordstrom D. K., Taylor H. E. and Kimball B. A. (2004) Rare earth element partitioning between hydrous ferric oxides and acid mine water during iron oxidation. *Appl. Geochem.* **19**, 1339–1354.
- Yates D. E. and Healy T. W. (1980) Titanium dioxide–electrolyte interface. Part 2. Surface charge (titration) studies. *J. Chem. Soc., Faraday Trans.* **76**, 9–18.
- Yoshida T., Ozaki T., Ohnuki T. and Francis A. J. (2004) Adsorption of rare earth elements by γ - Al_2O_3 and *Pseudomonas fluorescens* cells in the presence of deferroxamine B: implication of siderophores for the Ce anomaly. *Chem. Geol.* **212**, 239–246.
- Zhang Z., Fenter P., Cheng L., Sturchio N. C., Bedzyk M. D., Machesky M. and Wesolowski D. J. (2004a) Model-independent X-ray imaging of adsorbed cations at the crystal–water interface. *Surf. Sci.* **554**, L95–L100.
- Zhang Z., Fenter P., Cheng L., Sturchio N. C., Bedzyk M. D., Predota M., Bandura A. V., Kubicki J. D., Lvov S. N., Cummings P. T., Chialvo A. A., Ridley M. K., Benezeth P., Anovitz L., Palmer D. A., Machesky M. and Wesolowski D. J. (2004b) Ion adsorption at the rutile–water interface: linking molecular and macroscopic properties. *Langmuir* **20**, 4954–4969.
- Zhang Z., Fenter P., Cheng L., Sturchio N. C., Bedzyk M. J., Machesky M. L., Anovitz L. M. and Wesolowski D. J. (2006a) Zn^{2+} and Sr^{2+} adsorption at the TiO_2 (110)–electrolyte interface: influence of ionic strength, coverage, and anions. *J. Colloid Interf. Sci.* **295**, 50–64.
- Zhang Z., Fenter P., Kelly S. D., Catalano J. G., Bandura A. V., Kubicki J. D., Sofo J. O., Wesolowski D. J., Machesky M. L., Sturchio N. C. and Bedzyk M. J. (2006b) Structure of hydrated Zn^{2+} at the rutile TiO_2 (110)–aqueous solution interfaces: comparison of X-ray standing wave, X-ray absorption spectroscopy, and density functional theory results. *Geochim. Cosmochim. Acta* **70**, 4039–4056.

Associate editor: Karen Johannesson